OPTIMAL SELECTION OF SELF-PIERCING RIVETS FOR VEHICLE BODIES IN DIFFERENT APPLICATION ENVIRONMENTS

Anheng WANG[1, *], Tao WANG[1], Linran ZHU[1] and Jiang LI[2], Wentao ZHU[2]

Against the backdrop of the current development direction of automobiles tending towards lightweight, this paper reports a study of selecting self-piercing rivets for use in the assembly process of automotive white bodies. The C5.3-H4 type self-piercing rivets were selected as the research object to study the rivet sizes suitable for different arrangement and combination lapping of 2 mm and 3 mm aluminum plates. The stress and strain of self-piercing rivets during the entire riveting process were studied using finite element software. Finally, from experiments conducted to verify the findings, it is concluded that the optimal rivet length for the aforementioned sheet combinations is the sheet thickness plus 1.5–2 mm. It is also recommended to prioritize the use of thicker sheets as the bottom layer to achieve riveted joints that are more stable and reliable.

Keywords: Self-piercing riveting; Lightweight; Type selection recommendation; Finite element

1. Introduction

As an advanced cold-joining technology, self-piercing riveting (SPR) has demonstrated its unique advantages and broad application prospects in multiple industrial fields in recent years. SPR achieves mechanical connection by using specially made alloy steel rivets to penetrate the top sheet material directly without pre-drilling and form a non-penetrating cold deformation expansion in the bottom sheet material. Its unique connection mechanism makes SPR particularly suitable for connecting multi-layer, dissimilar, and composite materials, solving many bottlenecks in traditional connection processes. This technology not only enhances the safety performance of automobiles but also meets the requirements of the automotive industry for light weight, high strength, and high sealing.

Research on SPR to date has been focused primarily on the fatigue performance of joints and the prediction of forming quality, as the following

[1]School of Mechanical and Automotive Engineering, Anhui Polytechnic University, Wuhu 241000, China
[*]wahazf@ahpu.edu.cn
[2]Product Center of Research and Development Institute, Chery Automobile Co. Ltd., Wuhu 241000, China

examples show. Li et al. [1] investigated the impact of rivet distance from the sheet edge on joint forming quality. Zhao et al. [2] explored the relationship between joint fatigue life and the thickness of the riveted sheet, indicating that as the thickness of the thin sheet increases, the fatigue failure location shifts from the perforated thin sheet to the locking thin sheet. Huang et al. [3] examined the failure mechanism of riveted joints in a salt spray environment. Haque [4] focused on studying the influence of key factors such as the height of the rivet head, the remaining thickness of the base plate, and the effective interlocking value of the rivet in the base plate on the riveting forming effect. Moraes et al. [5] used nonlinear finite-element models and damage criteria sensitive to stress states to simulate and the influence of process parameters on the mechanical properties of riveted joints was studied in detail. Rusia and Weihe [6] compared the accuracies of different damage models and studied the influence of rivet installation depth on joint strength and failure mode; By comparing the geometric shape of the node with the cross-sectional view of the node and the force-displacement curve in the experiment, they provided an opportunity for intermediate verification of the numerical process. Wang et al. [7] conducted an in-depth study on the influence of lap joints made of different materials and pre-drilling of the upper layer plate on the forming quality, mechanical properties, failure modes and fracture characteristics of SPR joints in three-layer and multi-layer plates. Li et al. [8] studied the forming mechanism of friction SPR for high-strength sheet materials and low-ductility materials, as well as the influence of die parameters on the joint forming mechanism and forming quality. Ye et al. [9] researched the static mechanical properties and failure behavior of 5A06 aluminum alloy SPR joints after aging treatment, finding that the joint quality decreased significantly after one year of aging treatment. Zhang et al. [10] investigated the mitigation effect of spherical bottom dies on the cracking problem of low-ductility material base plates. Xue et al. [11] studied the additional strain and performance changes in the sheet material and rivet caused by SPR forming, obtaining more-accurate rivet material parameters to make finite-element simulation more precise. Mucha et al. [12] examined the influence of rigid punches and various deformable rivets on the joint forming quality. Cheng et al. [13] compared the effects of sheet thickness and pre-drilling hole diameter on the joint connection performance of traditional SPR and pre-drilled SPR. Zhang et al. [14] conducted research on joint parameters in steel–aluminum connections, discussing the effects of parameters such as punch diameter and punch chamfer on the mechanical properties of the joint. Xu [15] studied the influence of the physical parameters of the riveting die on the interlock value of the joint.

The above narrative shows a lack of research to date on rivet selection for different working conditions in industrial applications. Starting from the perspective of practical application and combined with existing riveting

equipment and mass-produced rivets, in this paper, finite element software is used for preliminary research, studies the same type of rivets with different specifications used in different plate lap situations, explores their optimal parameters, recommends the best matching selection, and provides certain guidance for actual production practice.

2. Three-dimensional numerical simulation

2.1 Creation of three-dimensional model for self-piercing riveting

The three-dimensional models used in this study were all created using Solidworks2022. SPR is a new type of cold-forming connection technology, the principle being that the riveting equipment presses rivets into two or three overlapping layers of sheet metal. With the cooperation of the bottom die, the rivet feet radiate and spread out to the surroundings, penetrate the upper sheet metal, and form fixed feet in the lower sheet metal, thereby achieving mechanical interlocking and sheet-metal connection. The models required for this process include punch, blank holder, rivet, upper sheet metal, lower sheet metal (and middle sheet metal if three layers are involved), and die, the three-dimensional modeling of which is shown in Fig. 1.

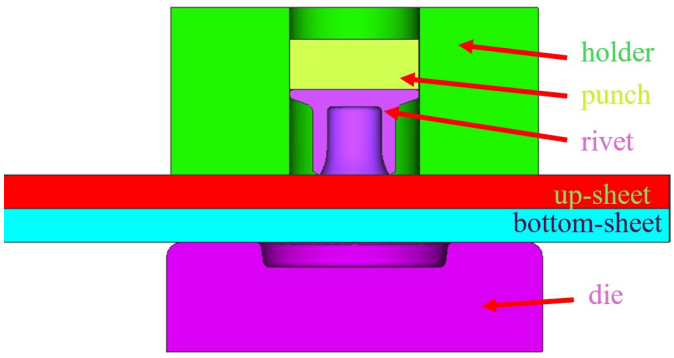

Fig. 1. Half of assembly model

2.2 Finite-element simulation of self-piercing riveting process

In the connections used for automotive white bodies, the aluminum–aluminum plate lap joint is used most commonly. This paper reports the use of the software Simufact Forming 16.0 to study the SPR of upper and lower aluminum plates with different thicknesses [11]. The material used for the upper and lower plates is DB.AlMgSi1 in the material library, which corresponds to the material properties of 6082 aluminum plate in China's national standard. The material of the finite element simulation rivets is 36MnB4, and the plate

material is AlMgSi1. Their material properties are shown in Table 1[9].

Table 1

Mechanical properties of materials

Name	Material	Elastic modulus [GPa]	Poisson's ratio	Density [kg/m^3]
DB.AlMgSi1	Al	69	0.25	2695
DB.36MnB4	Steel	210	0.29	7800

In the self-punching riveting simulation, the riveting gun punch, edge press frame and bottom mold are usually made of high-strength steel. In finite-element simulations, they are typically set as rigid bodies, ignoring their deformation, so there is no need to set material properties in the software. The press is defined manually, selecting a hydraulic device, setting the hydraulic type to a constant speed of 50 mm/s, and the punch pressure is 42–65 kN (depending on the different sheet thicknesses). The friction coefficient is defined manually, the friction criterion is set to "combined," referring to relevant literature, the Coulomb friction coefficient is set to 0.1 and the friction coefficient at the shear stress interface is 0.2. The temperature of the mold and the environment is 20°C, and the thermal conductivity is 50 W/(m ² ·K). Mesh refinement must be carried out for different parts. For example, rivets are assigned the Quadtree mesh type with a mesh size of 0.05 mm, while the upper and lower plates are set to Advancing Front Quad type with a mesh size of 0.1 mm. The forming control is selected as stroke-time control, with the direction being the negative Z-axis. Because the Simufact software has built-in contact types and analysis step settings, its solution process is simplifie.

2.3 Analysis of simulation results

2.3.1 Rivet leg length

Here, 2 mm + 2 mm aluminum plates are used for lap joints, with a rivet leg thickness of 0.85 mm, as shown in Fig. 2. It shows that with the rivet leg thickness unchanged, increasing the rivet leg length appropriately can effectively increase the interlock value. In the study of SPR performance, the size of the interlock value is related directly to the tensile strength of the joint. However, if the rivet leg length is too long, it will result in a small remaining value at the bottom of the joint or even penetrate the bottom layer of the plate, thereby increasing material consumption.

The parameters for evaluating the SPR forming effect are shown in Fig. 3 [12]. This article holds that when choosing self-piercing rivets in practical applications, the rivet length should be calculated as follows: rivet length = thickness of upper plate + thickness of lower plate + 1.5–2 mm.

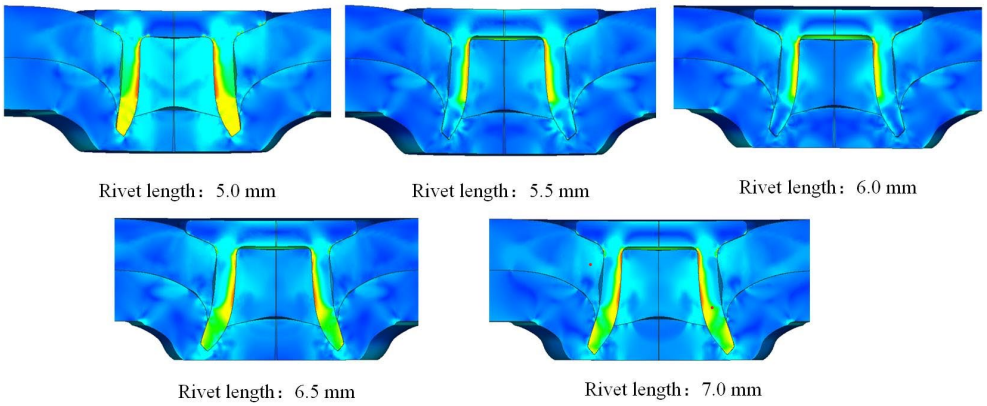

Fig. 2. Comparison of different rivet lengths

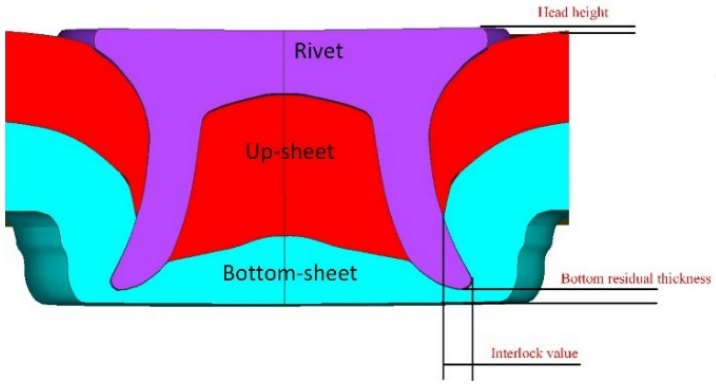

Fig. 3. Parameters for evaluation of riveting performance

2.3.2 Rivet leg thickness

In practical engineering applications, the design parameters of rivets directly affect the forming effect of joints. This paper selects a 2 mm + 2 mm plate lap joint with a rivet length of 5.5 mm to study the impact of rivet leg thickness on the forming effect of the connection point, the different results can be seen from Fig. 4. As can be seen, the thickness of the rivet leg has a small impact on the forming effect of the connection point. Therefore, when designing the rivet structure, the thickness of the rivet leg can be optimized appropriately to reduce material consumption.

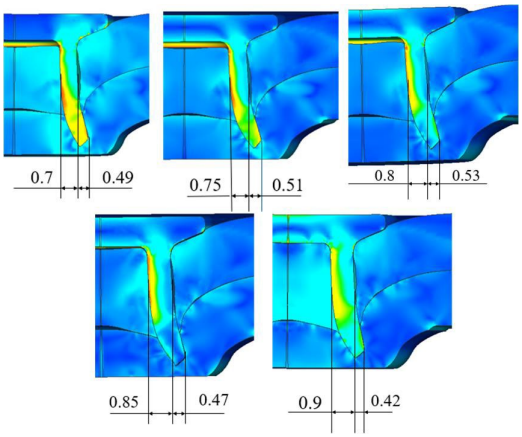

Fig. 4. Comparison of different rivet leg thicknesses

2.3.3 Plate thickness and rivet dimensions

The riveting dies used in this paper are flat-bottomed ones, with the upper and lower plate thicknesses set at 2 mm + 2 mm, 2 mm + 3 mm, 3 mm + 2 mm, and 3 mm + 3 mm, respectively. The length of the rivets starts at 5 mm and increases successively by 0.5 mm until the length increases to 7.5 mm. The degree of rivet leg spreading after riveting is shown in Fig. 5.

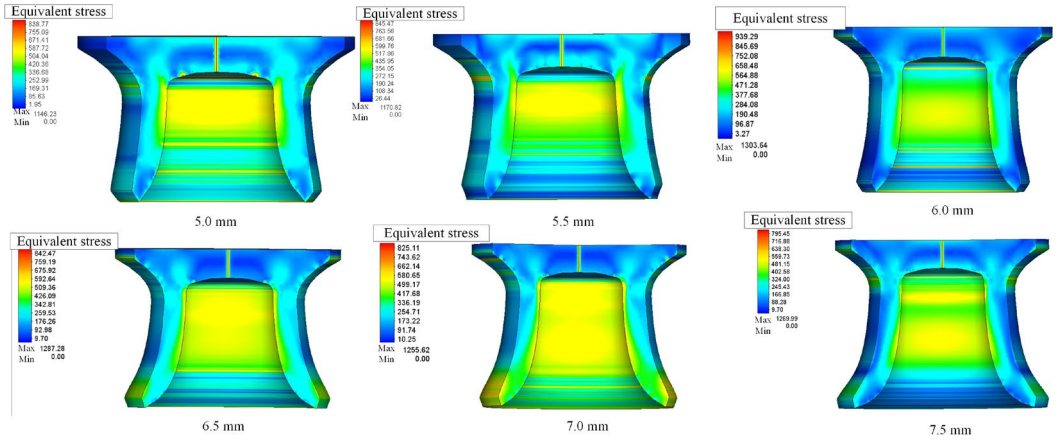

Fig. 5. Stress cloud map inside rivet after connection

From engineering experience, for the lap joints of two-layer plates, the rivet length should be greater than 1.5–2 mm of the total plate thickness. The finite-element simulation results are shown in Fig. 5, where the internal maximum stress is around 1500 MPa and the rivet leg is appropriate, which further verifies the rationality of the conclusion of 2.3.1 in this chapter.

3. Tests of lap joints formed by self-piercing riveting

To verify the rationality of using rivets of different lengths in different situations involving plate lap joints as discussed in Sec. 2, experimental verification was designed in this study.

3.1 Test of self-piercing riveting

The experiment involved four types of plate lap joint [16]: 2 mm + 2 mm, 2 mm + 3 mm, 3 mm + 2 mm, and 3 mm + 3 mm. For the riveting, among the C5.3-H4 rivets with the same diameter but different lengths, select rivets with lengths ranging from 5.0 mm to 7.5 mm [17]. The shear strength of the riveted joints was tested, and their key cross-sectional parameters were measured to further explore the impact of rivet leg length on joint performance. The plates used in this experiment were 6082-T6 aluminum plates [5] with the specifications of 105 mm × 45 mm × 2 mm and 105 mm × 45 mm × 3 mm. The stamping equipment was the RIVSET® Automation E installation system (Böllhoff), with a riveting speed of 50 mm/s and a punch pressure of 42–65 kN (the press riveting force must be increased appropriately for different rivet lengths). The riveting die is a flat-bottomed riveting die, with a relatively shallow die depth of 1.5 mm and a diameter of 11 mm. All the riveting results are shown in Fig. 6.

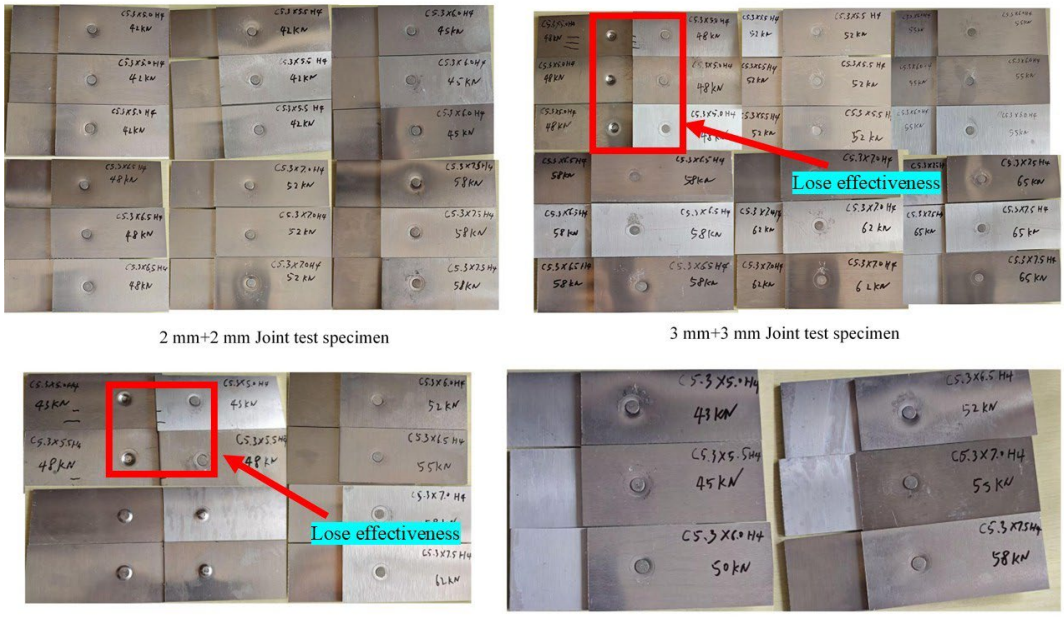

2 mm+2 mm Joint test specimen

3 mm+3 mm Joint test specimen

3 mm+2 mm Joint test specimen

2 mm+3 mm Joint test specimen

Fig. 6. Riveting test specimens

During the actual riveting process, it was found that when using

5.0-mm-long rivets, as shown in Fig. 6, when a 2 mm aluminum plate is placed below a 3 mm aluminum plate and overlapped with two 3 mm plates, effective riveting cannot be achieved. After observing the failed riveted joint through the test, it was found that the rivets did not penetrate the upper aluminum plate, thus failing to form an effective connection. However, rivets of the same type achieved effective riveting for the 2 mm + 3 mm plate lap configuration. This indicates that the lap configuration of the plates has a significant impact on the riveting effectiveness, and this factor should be considered in actual production and assembly processes.

3.2 Analysis of cross-sectional morphology

Taking the 2 mm + 2 mm aluminum plate lap joint as an example, C5.3-H4 rivets with lengths of 5–7.5 mm were used for riveting, with the same type of riveting die used for consistency. To ensure reliable connection, the specimens for cross-sectioning were double-riveted, as shown in Fig. 7. After riveting, we observed and measured the joint cross-section and mapped the key parameters of the connection points, and the results are shown in Fig. 8.

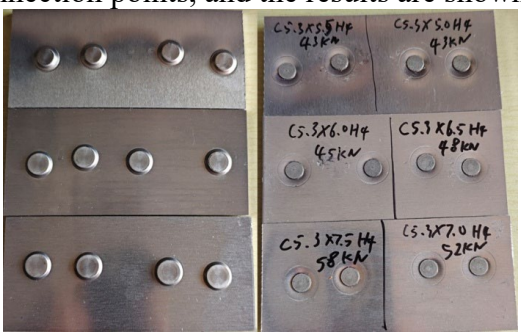

Fig. 7. Test specimens for double-rivet connection

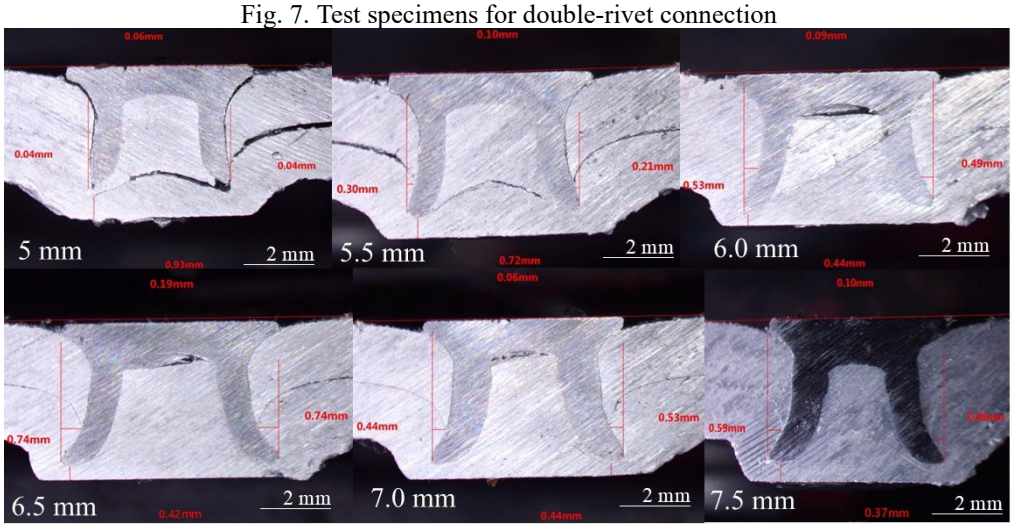

Fig. 8. Images of joint cross-section

According to the relevant quality standard document of the Böhler & Schaurte company for SPR joint points, for the C5.3-H4 rivet in a two-layer plate lap joint, after forming, the head height should be controlled between −0.2 mm and 0.3 mm, the residual thickness at the bottom should be greater than or equal to 0.15 mm, and the left and right interlock value should be greater than or equal to 0.12 mm. Fig. 9(a) shows an actual cross-sectional screenshot of the joint and the simulation results [18], and Fig. 9(b) shows the key parameters of the joint obtained from this experiment. According to the data in Fig. 9(b), when the length of the rivet increases, in order to control the height of the rivet head within a certain range, it is necessary to achieve this effect by adjusting the parameters of the riveting machine. The left–right interlock value increases and then decreases, while the remaining amount at the bottom decreases gradually [19]. All these results meet the industry requirements.

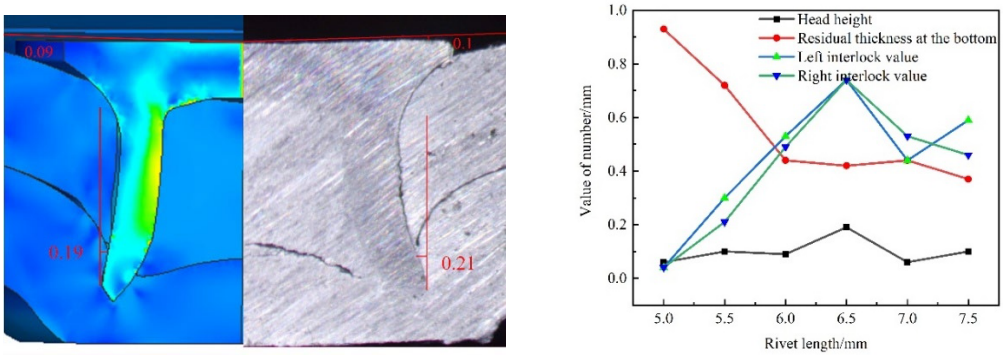

(a) Cross-sectional comparison diagram (b) Key parameters of joint

Fig. 9. Data for key cross-section parameters

3.3 Static tensile test

To investigate the quality of joint riveting, this paper reports the use of a universal tensile testing machine to perform shear tensile experiments on four types of lap-joint specimens after riveting [20], as shown in Fig. 10.

For a plate lap with an upper layer thickness of 3 mm and a lower layer thickness of 2 mm and a plate lap with an upper layer thickness of 3 mm and a lower layer thickness of 3 mm, the 5.5 mm long rivets cannot penetrate the upper plate to form an effective interlock, so the tensile test cannot be performed.

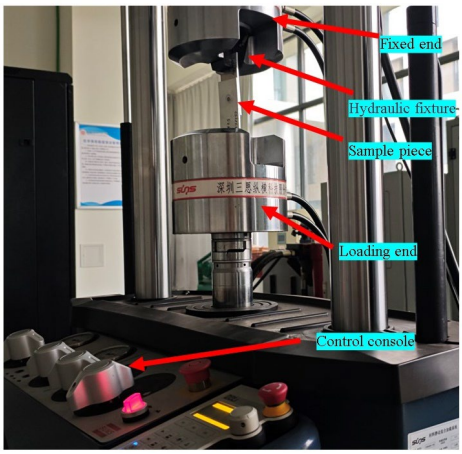

Fig. 10. Shear experiment

Fig. 11 shows the tensile-strength curves of each lap-joint combination ("2 mm+2 mm-5.0 mm" indicates that the thickness of the upper aluminum plate is 2 mm, the thickness of the lower aluminum plate is 2 mm, and the length of the rivet used is 5 mm. The same applies below.).

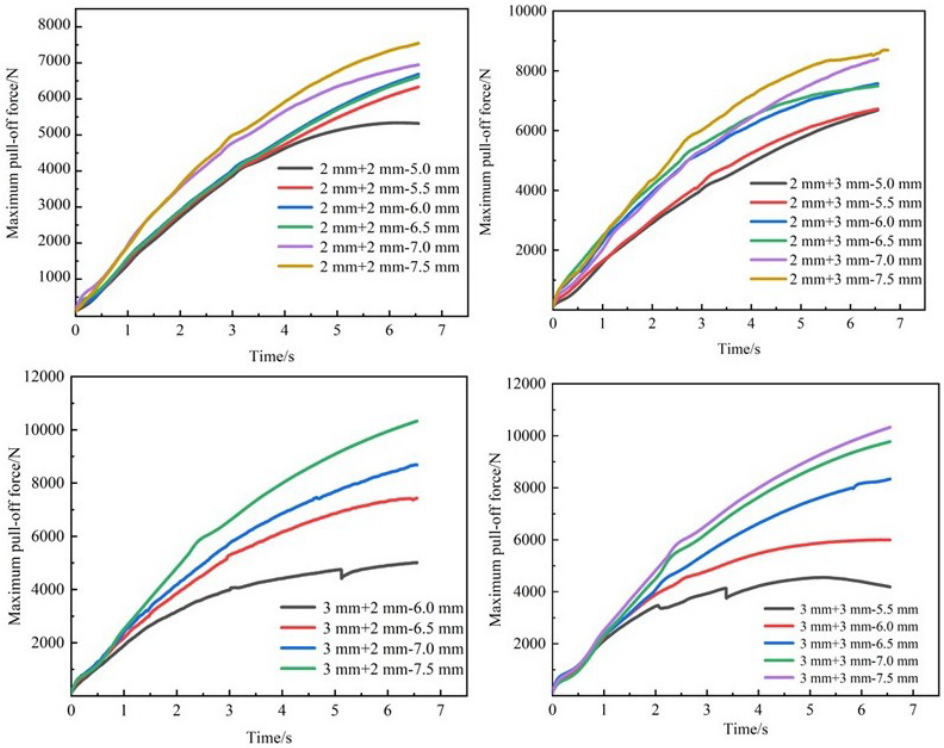

Fig. 11. Experimental data of joint shear tensile test

Fig. 11 shows that under the premise of forming effective riveting, the joint tensile strength increases with increasing rivet length. In practical production, it is advisable to place the thicker plate on the bottom to form effective riveting, and the rivet length is recommended to be the plate thickness plus 1.5–2 mm.

4. Theoretical analysis of connection point failure

Self-piercing riveted joints are limited by their connection form, resulting in various internal stresses at the connection point, such as shear stress during rivet insertion and yield stress during plate deformation. Due to the offset of half the plate thickness on the centerlines of the upper and lower plates, a bending moment M exists at the connection point. The joint fails under the combined action of multiple forces. The entire pull-out process is shown in Fig. 12.

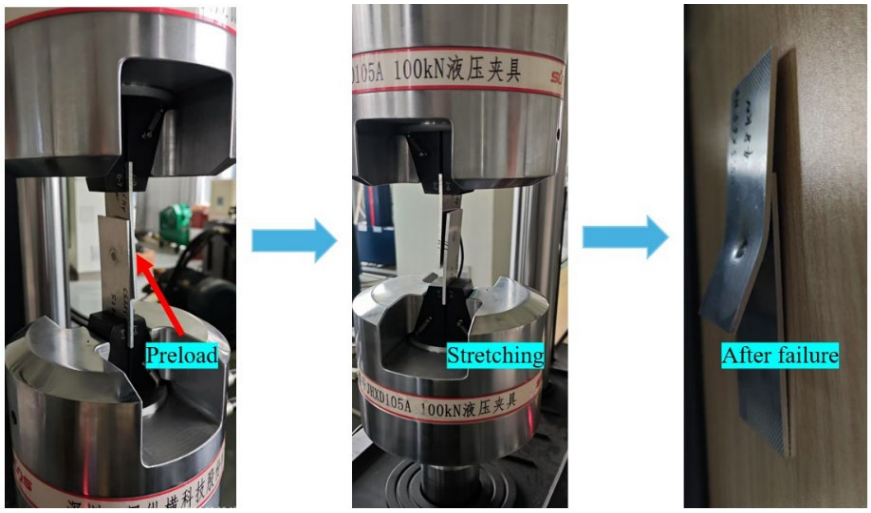

Fig. 12. Shear tensile testing process

To study its specific numerical values, the calculation formula [9] is provided here, where the calculation formula for bending moment is:

$$M = F_s \Delta t \tag{1}$$

Among them: M represents the bending moment, F_s represents the tensile force of the plate along the Z-axis, and Δt represents the center distance between the two aluminum plates in the Z-axis direction.

During the entire tensile test, the connection point deforms under the action of tensile force F_s, rivet shear force τ_r, and plate tensile stress σ_s, ultimately leading to connection point failure. The specific calculation relation is as follows:

$$F_f = (Min)\begin{cases} \dfrac{B_1 t_1^{\,2}}{4}\sigma_{S1} + \dfrac{B_2 t_2^{\,2}}{4}\sigma_{s2} \\ \tau_r A \\ (B_1 - \phi r)t_1\sigma_{s1} \\ (B_2 - \phi r)t_2\sigma_{s2} \end{cases} \tag{2}$$

Among them: F_f represents the joint failure force, B_1, B_2 represents the width of the upper and lower plates, t_1, t_2 represents the thickness of the upper and lower plates, σ_{s1}, σ_{s2} represents the yield stress of the upper and lower plates, τ_r represents the shear stress of the rivet joint cross-section, A represents the cross-sectional area of the rivet, ϕ_r represents the inner diameter of the rivet leg.

During the tensile process, the connection point will fail at the weakest point. The first equation represents the deformation of the plate at the connection point and the rivet being pulled out. The second equation indicates that the rivet is directly broken at the connection point. The third and fourth equations represent the upper and lower plates being directly broken. In this experiment, all connection points failed due to plate deformation and rivet pull - out. As shown in Fig. 13.

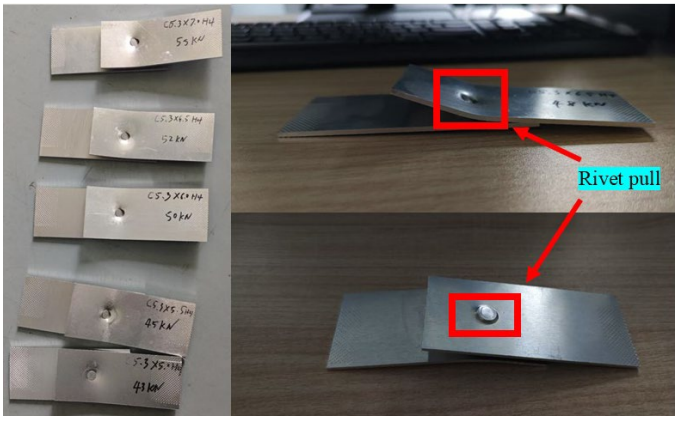

Fig. 13. Results of connection point failure

However, the calculation results according to the above formula show that the weakest point is that the rivet is directly sheared off, which does not conform to the actual experimental situation. Therefore, it is necessary to further study the force situation of the joint point. Here, it is necessary to consider that under the action of the bending moment *M*, the joint point will cause the upper and lower plates of the joint to bend and deform, and the force situation at the joint point is shown in Fig. 14.

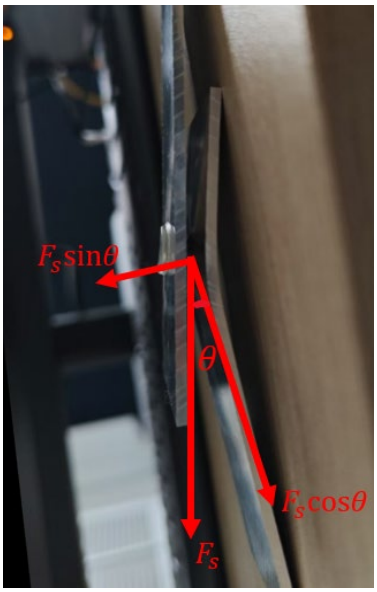

Fig. 14. Force situation of the joint point

In the figure, θ represents the included angle of the plate after deformation, $F_s\cos\theta$ represents the shear force along the plate, and $F_s\sin\theta$ represents the tensile force in the horizontal direction. Combining with Relation (2), it can be known that the shear failure force F_{fy} in the vertical direction is calculated as shown in Relation (3):

$$F_{fy}=\min\begin{cases}\dfrac{\tau_r A}{\cos\theta}\\ \dfrac{(B_1-\phi r)t_1\sigma_{s1}}{\cos\theta}\\ \dfrac{(B_2-\phi r)t_2\sigma_{s2}}{\cos\theta}\end{cases} \tag{3}$$

The tensile force F_{fx} in the horizontal direction is shown in Relation (4).

$$F_{fx}=(\min)\begin{cases}\sum\mu\sigma_{1s}A_{1s}+f_h\\ \sum\mu\sigma_{2s}A_{2s}+f_i\end{cases} \tag{4}$$

F_{fx} represents the tensile force in the X-axis direction, and μ represents the friction coefficient between the rivet surface and the cross-section of the aluminum plate, σ_{1s} represents the internal stress in the upper plate after riveting, σ_{2s} represents the internal stress in the lower plate after riveting, A_{1s}

represents the contact area between the upper plate and the rivet, A_{2s} represents the contact area between the lower aluminum plate and the surface of the rivet. f_h represents the resistance of the rivet head, and f_i represents the interlocking force after the rivet is embedded in the bottom plate.

The final failure judgment of the joint point can be obtained by calculation using Relation (5):

$$F_f = \begin{cases} F_{fy} \cos\theta \\ F_{fx} \sin\theta \end{cases} \tag{5}$$

Combining simulation results, experimental data and theoretical formulas, it can be known that as the rivet length increases, the contact area between the surface of the rivet and the internal sections of the upper and lower plates increases, and the tensile pull - off force of the joint point increases (that is, the tensile strength of the joint point increases). However, the increase in rivet length will gradually reduce the residual bottom thickness. In order to ensure a certain bottom residual thickness, joint experiments need to be carried out before formal production to ensure that the selected rivet model meets the design standards.

5. Results and Discussion

For the lap joints of the four plate combinations, Fig. 15 shows their maximum pull-off force after riveting with rivets of different lengths. The results show that for the lap joints of a given plate combination, the maximum pull-off force increases with increasing rivet length.

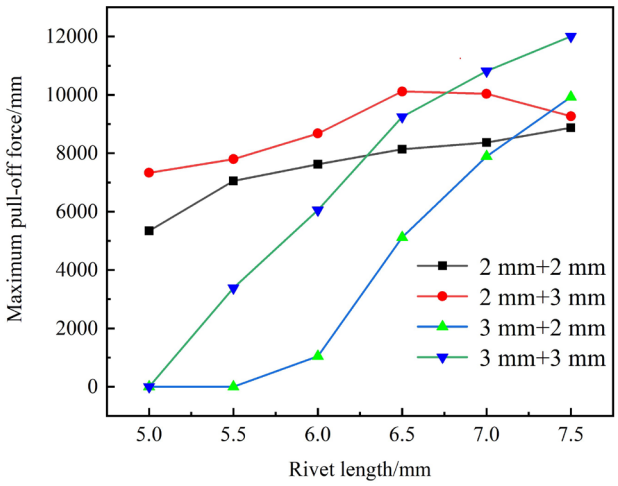

Fig. 15. Maximum pull-off force for each joint

The joint strength is directly related to the key parameters of the joint after SPR, and finite-element simulation and experimental measurement produced the graph of those key parameters shown in Fig. 16. The experimental and simulation data show that as the rivet length increases, the interlock value increases then decreases and finally stabilizes, and the residual thickness at the bottom decreases gradually. For some cases with special requirements on the sealing performance of the joint [21-22], sufficient residual thickness at the bottom must be ensured.

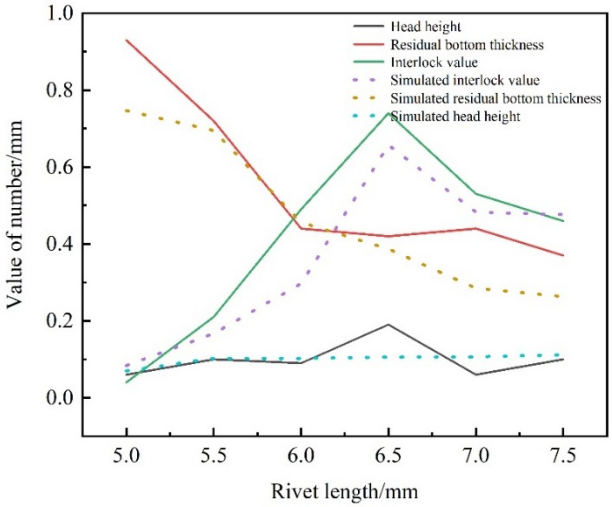

Fig. 16. Comparison chart of key parameters of joint

6. Conclusions

Through the application of finite element software and actual experiments, the influence of various aluminum plate lap joint methods on the riveting effect were investigated. Experiments were conducted on the specimens during the riveting process and after the riveting. The conclusions are as follows:

1. For aluminum-aluminum sheet lapping, it is recommended to prioritize placing the thicker aluminum sheet at the bottom to enhance the feasibility and strength of the connection.
2. During the self-piercing riveting process, the wall thickness of the rivet leg has a relatively small influence on the quality of the joint. When designing the rivet structure, it is feasible to consider reducing the wall thickness of the rivet leg appropriately to improve economic viability.
3. Among the critical parameters of SPR, the interlocking value has the greatest influence on the mechanical properties of the connection point. With the premise of ensuring sufficient residual bottom thickness, within a certain range, the interlocking value increases with the increase of the length of the rivet leg. Based on the above simulation and the analysis of the experimental results, the

recommended length of the rivet leg is the total thickness of the plate layer plus 1.5-2 mm.

Authors' contributions

Tao Wang: Data curation, Formal analysis, Software, Writing - original draft, Writing - review & editing. Anheng Wang: Conceptualization, Methodology, Funding acquisition, Supervision, Writing - original draft. Linran Zhu: Data curation, Investigation, Resources, Validation. Jiang Li: Conceptualization, Project administration, Validation. Wentao Zhu: Methodology, Resources, Visualization, Investigation.

Acknowledgments

The authors gratefully acknowledge the support of Anhui Ruixiang Industry Co., Ltd. in the experiment.

REFERENCES

[1] *Li, D., Han, L., Thornton, M., & Shergold, M.,* Influence of edge distance on quality and static behaviour of self-piercing riveted aluminium joints. Materials and Design, vol.34, pp.22-31, 2012.Doi:10.1016/j.matdes.2011.07.046

[2] *Zhao, L., He, X., Xing, B., Lu, Y., Gu, F., & Ball, A.,* Influence of sheet thickness on fatigue behavior and fretting of self-piercing riveted joints in aluminum alloy 5052. Materials & Design, vol.87, pp.1010-1017, 2015. Doi 10.1016/j.matdes.2015.08.121

[3] *Huang, Z. C., Jia, Y. L., Jiang, Y. Q., & Zhang, Y. C.,* Mechanical properties and fatigue failure mechanisms of purely self-piercing riveted (SPR) and hybrid (SPR-bonded) joints under salt spray environment. Journal of Materials Research and Technology, vol.20, pp.2501-2517, 2022. Doi10.1016/j.jmrt.2022.08.024

[4] *Haque, R.,* Quality of self-piercing riveting (SPR) joints from cross-sectional perspective: A review. Archives of Civil and Mechanical Engineering, vol.18, no.1, pp.83-93, 2018. Doi 10.1016/j.acme.2017.06.003

[5] *Moraes, J. F. C., Jordon, J. B., Su, X., Barkey, M. E., Jiang, C., & Ilieva, E.,* Effect of process deformation history on mechanical performance of AM60B to AA6082 self-pierce riveted joints. Engineering Fracture Mechanics, vol.209, pp.92-104, 2019. Doi 10.1016/j.engfracmech.2018.12.020

[6] *Rusia, A., & Weihe, S,* Development of an end-to-end simulation process chain for prediction of self-piercing riveting joint geometry and strength. Journal of Manufacturing Processes, vol.57, pp.519-532, 2020.Doi 10.1016/j.jmapro.2020.07.004

[7] *Wang, C., Yu, W., Cheng, A., & He, Z.,* Study on the failure mechanism and mechanical properties of multi-layer hole-drilled self-piercing riveted three-layer steel/aluminum hybrid joints. Engineering Failure Analysis,vol.164, pp.108681, 2024. Doi 10.1016/j.engfailanal.2024.108681

[8] *Li, Y., Lim, Y. C., & Feng, Z.,* Effect of die design on microstructure and mechanical joint strength in friction self-piercing riveted AA7055-T76 and AA7055-T76. Journal of Manufacturing Processes, vol.124, pp.119-130, 2024. Doi 10.1016/j.jmapro.2024.06.005

[9] *Ye, K., Zhao, L., Abbas, Z., Li, C., Liu, G., Lei, L., Islam, M. S.,* Static mechanical properties and failure behaviors of self-piercing riveted joints in aluminum alloy 5A06 after aging. Thin-Walled Structures, vol.201, no. Part B, pp.112041, 2024. Doi 10.1016/j.tws.2024.112041

[10] *Zhang, A., Zhao, L., Li, L., Abbas, Z., Li, J., Shao, Y., Monier, A.,* Effect of die designed geometrical parameters on riveting quality of self-piercing riveting joints in 5052 aluminium alloy. Scientific Reports, vol.15, no.1, pp.7239, 2025. Doi 10.1038/s41598-025-92142-1

[11] *Xue, Z., Wang, X., Xu, C., Chen, Z., Feng, X., Zhou, Q., Li, L.,* Equivalent characterization of pre-strained material properties and mechanical behavior prediction of steel/aluminum self-piercing riveted joints. Thin-Walled Structures, vol.182, no. Part B, pp.110243, 2023. Doi 10.1016/j.tws.2022.110243

[12] *Mucha, J., Boda, Ł., & Witkowski, W.,* Geometrical parameters and strength of clinching joint formed with the use of an additional rivet. Archives of Civil and Mechanical Engineering, vol.23, no.2, pp.114, 2023. Doi 10.1007/s43452-023-00653-3

[13] *Cheng, A., Wang, C., Sun, Y., & Luo, G.,* Effects of hole sizes and stack thicknesses on mechanical properties and failure behavior of pre-holed self-piercing riveted steel-aluminum joints. Journal of Materials Engineering and Performance, 2024. Doi 10.1007/s11665-024-09767-y

[14] *Zhang, Y., Liao, C., Wang, T., Xu, C., Peng, J., Lei, B., & Jiang, J.,* Steel-aluminum clinched joints mechanical properties and strength prediction under different geometric parameters. Journal of Constructional Steel Research, vol.226, pp. 109196, 2025. Doi 10.1016/j.jcsr.2024.109196

[15] *Xu, Y.,* Effects of factors on physical attributes of self-piercing riveted joints. Science and Technology of Welding and Joining, vol.11, no.6, pp.666-671, 2006. Doi 10.1179/174329306x131866

[16] *Wu, J., & Chen, C.,* Influence of thickness combinations on mechanical properties of joints produced by clinch riveting with rigid rivet. The International Journal of Advanced Manufacturing Technology, vol.121, no.11,pp. 7907-7921, 2022. Doi 10.1007/s00170-022-09704-0

[17] *Kim, C., Min, K. M., Choi, H., Kim, H. J., & Lee, M. G.*, Development of analytical strength estimator for self-piercing rivet joints through observation of finite element simulations. International Journal of Mechanical Sciences, vol.202-203, pp.106499, 2021. Doi 10.1016/j.ijmecsci.2021.106499

[18] *Porcaro, R., Hanssen, A. G., Langseth, M., & Aalberg, A.,* Self-piercing riveting process: An experimental and numerical investigation. Journal of Materials Processing Technology, vol.171, no.1 pp.10-20, 2006. Doi 10.1016/j.jmatprotec.2005.05.048

[19] *Hoang, N. H., Hopperstad, O. S., Langseth, M., & Westermann, I.,* Failure of aluminium self-piercing rivets: An experimental and numerical study. Materials & Design, vol.49, pp.323-335, 2013. Doi: 10.1016/j.matdes.2013.01.034

[20] *Kim, D.Y., Kim, D.O., Cheon, S.S.,* Experimental investigation on fatigue characteristics of SPR (Self-Piercing Rivet) and hybrid joints. Journal of the Korean Society for Precision Engineering, vol.35, no.3, pp.335-340, 2018. Doi 10.7736/kspe.2018.35.3.335

[21] *Porcaro, R., Hanssen, A. G., Langseth, M., & Aalberg, A.,* The behaviour of a self-piercing riveted connection under quasi-static loading conditions. International Journal of Solids and Structures, vol.43, no.17, pp.5110-5131, 2006. Doi 10.1016/j.ijsolstr.2005.10.006

[22] *Ma, Y., Lou, M., Li, Y., & Lin, Z.,* Effect of rivet and die on self-piercing rivetability of AA6061-T6 and mild steel CR4 of different gauges. Journal of Materials Processing Technology, vol.251, pp. 282-294, 2018. Doi 10.1016/j.jmatprotec.2017.08.020